

Detecting Road Obstacles by Erasing Them *

Krzysztof Lis Sina Honari Pascal Fua Mathieu Salzmann

Computer Vision Laboratory, EPFL

Abstract

Vehicles can encounter a myriad of obstacles on the road, and it is impossible to record them all beforehand to train a detector. Instead, we select image patches and inpaint them with the surrounding road texture, which tends to remove obstacles from those patches. We then use a network trained to recognize discrepancies between the original patch and the inpainted one, which signals an erased obstacle.

We also contribute a new dataset for monocular road obstacle detection, and show that our approach outperforms the state-of-the-art methods on both our new dataset and the standard Fishyscapes Lost & Found benchmark.

1. Introduction

Modern methods provide a nearly complete toolkit for vision-based autonomous driving. That includes road segmentation [9, 34], lane-finding [29, 37], vehicle and pedestrian detection [39, 13, 6], and multi-class semantic [51, 8, 40], instance [18] and panoptic [23, 47] segmentation. Moreover, vision-based assistance is now widely accepted in the market [1] and enables vehicles to plan a path within the predicted drivable space while avoiding other traffic participants. However, the risk of missing strange and unexpected obstacles lying on the road remains. Such obstacles are as rare as they are diverse, which prevents direct application of the now standard approach of training deep networks by showing them an exhaustive set of annotated samples.

In practice, detecting such unexpected obstacles often requires LiDAR sensors [43] or multiple cameras [36]. Here, we propose instead a method that only needs a single RGB image to detect obstacles in



Figure 1. **Detecting unexpected obstacles in good and bad weather.** **Top:** Objects one would not expect to see on a road and that are not featured in standard databases. **Middle:** The road area has been inpainted. **Bottom:** After comparing the original and inpainted images, our discrepancy network returns a binary mask that denotes the obstacle locations.

the drivable area, under the assumption that objects outside that area are irrelevant because a self-driving car will detect the road before planning to drive and will not leave the drivable area of its own accord. To demonstrate this to be a viable assumption, we will show results given either the ground-truth location of the road edges or only an imperfect road segmentation produced by an off-the-shelf segmentation algorithm.

Our approach relies on the fact that obstacles look different from the surrounding road surface. We thus detect them by inpainting image-patches using their surroundings and then checking how similar the inpainted patch is to the original one. While a similar intuition has been used to detect anomalies in several application scenarios, such as detecting manufacturing defects [50, 17] or anomalous faces [4], the very constrained nature of these tasks made it possible to rely

*This work was supported in part by the International Chair Drive for All - MINES ParisTech - Peugeot-Citroën - Safran - Valeo.

on simple comparisons of handcrafted features. By contrast, on roads, this would yield many false positives due to road markings, diversity in road texture, and obstacles extending beyond the inpainted patch.

Our solution is to introduce a *discrepancy network* trained to recognize which differences between the inpainted patch and the original one are significant. It returns a per-pixel heatmap denoting the presence of obstacles. To train it to handle objects that are *not* part of the training database, we generate samples featuring synthetic obstacles by moving existing training objects, such as road signs and people, onto the road.

Our experiments show that our discrepancy network trained solely on Cityscapes [10] objects successfully detects obstacles on images depicting significantly different road scenes, without requiring any annotated data nor any re-training for these new scenes. In other words, our method generalizes well to previously unseen real obstacles and new road surfaces. It outperforms earlier monocular road anomaly detectors [28, 5, 30, 3] on the *Lost & Found* [36] data featured in the *Fishyscapes* benchmark [5], as well as on our own newly collected dataset featuring additional unusual objects and road surfaces.

Our contribution is therefore a simple but effective approach to detecting obstacles that never appeared in any training database, given only a single RGB image. We also contribute a new dataset for evaluating anomaly detection models. We will make our obstacle detection code¹, our semi-synthetic training dataset, and our new benchmark dataset² publicly available.

2. Related Work

In this section, we briefly review methods that, as ours, rely on a single RGB image for obstacle detection and do not use explicit obstacle training sets. For a more complete survey of obstacle detection algorithms, we refer the reader to [36, 38, 15, 48].

2.1. Image Reconstruction for Anomaly Detection

If an image is reconstructed so as to preserve the appearance in normal regions and discard anomalous ones, those anomalies can be detected by comparing the input to the reconstruction. This has been achieved in several ways we now discuss.

In [2], the distribution of inlier images is modeled by training an autoencoder, followed by a feature comparison between the input and reconstruction. Auto-encoding has been used to find highway obstacles

in [11, 33], where input patches are passed through a Restricted Boltzmann Machine. Its limited expressive power is supposed to preserve the smooth road surface while altering obstacles. This approach, however, does not address textured road surfaces. As opposed to encoding the input image, the method of [41] trains a generator to capture the training distribution and searches for a latent vector producing an image most similar to the input. However, this method operates on microscopic scans of tissue samples, and, to our knowledge, it has not been applied to data with distributions as diverse as outdoor road scenes.

Other methods [28, 46] explicitly restrict the intermediate representation of the scene to a dense semantic map, and synthesize a plausible matching image using conditional GANs for image translation [19, 45]. Since the anomalous regions are not represented by the typical semantic classes, their appearance will be altered by this process. In [28], the input and synthesized images are compared using a learned discrepancy module, while [46] uses a feature distance measure.

Rather than encoding the input, one can remove parts of the image and inpaint them based on the surrounding context. In [17] square patches are inpainted and compared with an L_1 metric to detect material defects; the method of [50] combines the reconstructions obtained with a set of random inpainting masks and uses a multi-scale gradient magnitude similarity metric for comparison. In the context of road scenes, [32] proposes to compare the road appearance to similar images memorized from previous video frames; however this would lead to false positives when entering an area with a new road texture. Furthermore, these methods assume high fidelity of the reconstruction, and detect every visible difference as an anomaly. In outdoor scenes with road markings and diverse surface textures, the inpainting is bound to be imperfect. We address this by training a discrepancy network to focus on the relevant differences.

2.2. Anomaly Detection in Semantic Segmentation

The problem of detecting anomalies can be posed as one of open-set semantic segmentation. With standard, fully-supervised semantic segmentation networks, all pixels, including the anomalous ones, will be classified into one of the training semantic categories. Open-set semantic segmentation then aims to find the outliers in the resulting semantic maps. The method of [3] introduces an outlier detection head sharing backbone features with the semantic segmentation one. It is trained using extensive out-of-distribution data, injecting outlier patches drawn from ImageNet-1k [12] into the Cityscapes and Vistas [35] scenes.

¹ Code and semi-synthetic training set:
github.com/cvlab-epfl/erasing-road-obstacles

² *Road Obstacles* dataset:
www.epfl.ch/labs/cvlab/data/road-obstacles-2021

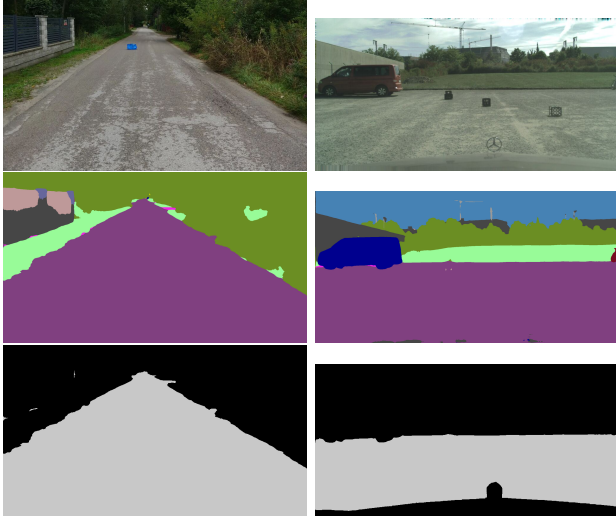


Figure 2. **Drivable space from semantic segmentation.** **Top:** Input images. **Middle:** Semantic segmentation by PSP-Net [51]. The class colors follow Cityscapes convention. **Bottom:** We take the drivable space to be the union of the *road* (purple) and *sidewalk* (magenta) pixels, excluding the known ego-vehicle mask. Obstacles visible in the input image have been classified as part of the road by the segmentation algorithm and our extra obstacle detection step is needed to find them.

The work of [5] proposes to learn the inlier distribution of features extracted from a layer of the semantic segmentation network. It uses a normalizing flow to bijectively map the features to latent vectors following a Gaussian distribution. The mapping is trained to maximize the likelihood of the features observed in inlier samples.

Another approach involves estimating the uncertainty of label prediction based on the assumption that outlier regions should yield low classification confidence. Bayesian deep learning treats the network weights and outputs as probability distributions. In practice, dropout [44] is used to approximate the distribution over model weights, applied to semantic segmentation in [20, 21]. Alternatively an ensemble of networks can be used [25, 16]. In [30], the Dirichlet differential entropy is used as a measure of uncertainty. We find that the performance of these statistical methods as obstacle detectors degrades significantly when faced with road surfaces differing from the training set, as the novel textures are treated as anomalies. We will show that our approach based on comparing the original image with an inpainted one with a discrepancy detector does not suffer from this drawback.

3. Approach

Our goal is to identify obstacles that are on the road, whose extent is typically computed by a previous stage in the self-driving perception pipeline that is tasked with detecting the drivable area. To simulate that stage we use either the semantic segmentation network of [51] trained on the Cityscapes dataset [10] or the actual ground-truth data for the road location. Hence, we operate under the assumption that the system installed in a real car would have performances intermediate between the two. As shown in Fig. 2, we should then look for undetected obstacles within the supposedly drivable area, and this is where our method comes in. We chose this scenario because this is the one that truly requires obstacle detection, unlike situations in which the system fails to detect the road. In such cases, the vehicle would simply not plan a path through the area.

In other words, our chosen task is to identify all pixels, within that estimated road area, that denote obstacles. This is difficult because obstacles can take many forms. Furthermore, because they are unexpected, there is no guarantee that they were present in the database used to train a network to recognize them. Hence, the network must be made to respond to *objects that does not belong to the road* without any clear description, or even exemplars, of these objects.

To this end, given a binary mask denoting the drivable area in the image, we propose the following two-step approach:

1. Erase the obstacles by removing road patches and inpainting them in a sliding-window manner;
2. Use a discrepancy network to compare the original image to the inpainted one and decide if they are similar enough.

The intuition behind this scheme is that, if there is an obstacle, the inpainted area will look very different from the original image. However, even if there is no obstacle, the inpainted area will be similar to the original one, but not strictly equal. Hence, the discrepancy network is needed to assess if they are dissimilar enough to flag a potential obstacle. It yields a heatmap denoting the likelihood for each pixel in the drivable area of belonging to an obstacle. In the remainder of this section, we discuss these two steps in more details.

3.1. Inpainting

To erase the obstacles while preserving the surrounding road appearance, we use a general-purpose inpainter [49] that relies on an adversarial approach to ensure that the inpainted image looks realistic. We use

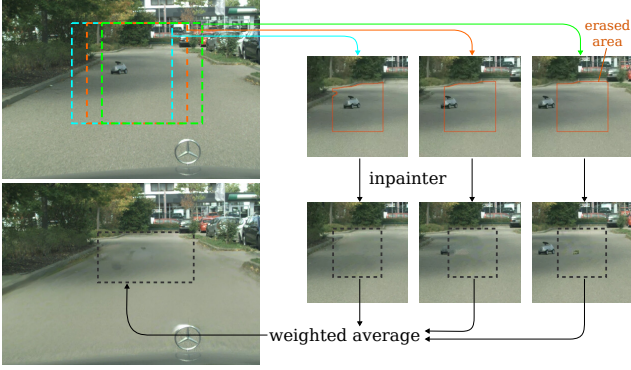


Figure 3. **Sliding window inpainting of the road surface.** We extract 400×400 context patches then erase and inpaint the road area contained within the central 200×200 of the patch. Finally we fuse the inpaintings which reconstructs the road appearance while removing localized obstacles. Note how the process was able to preserve the shadow of the trees.

a version of this model trained on the scene recognition dataset Places2 [52], and do not train it further.

A naive way to use it would be to inpaint the entire road area at once. This, however, would provide no indication to the inpainter of the road appearance, leading to inpainted images that differ from the original ones in the whole road region, thus precluding subsequent obstacle detection. Instead, we inpaint road patches to provide sufficient context for the network to reconstruct the road surface, as shown in Fig. 3. The patches nonetheless need to be large enough to encompass obstacles whose size we do not know *a priori*. We therefore follow a sliding-window approach, inpainting patches of 200×200 pixels of drivable area within 400×400 image regions to provide context.

While an obstacle is usually nicely erased when the area to inpaint encloses it completely, the inpainter is able to re-create the obstacles that are only partially contained in the inpainted region. To resolve this, we use consecutive patches with a relative overlap of 0.7, increasing the likelihood of having at least one patch that covers the entire obstacle. This means that each image pixel is inpainted multiple times. We then fuse the multiple inpaintings of each pixel by weighted averaging, where the weight of each inpainting is computed based on the Manhattan distance between the corresponding patch center and the pixel location of interest. Formally, a patch centered at location $\mathbf{c}_j = [u_j, v_j]^\top$ contributes to the inpainting of a pixel at location $\mathbf{p} = [u, v]^\top$ with a weight

$$w = \frac{1 - \frac{2}{s} \max(|u - u_j|, |v - v_j|)}{\sum_{[u_i, v_i] \in \Pi(u, v)} 1 - \frac{2}{s} \max(|u - u_i|, |v - v_i|)}, \quad (1)$$

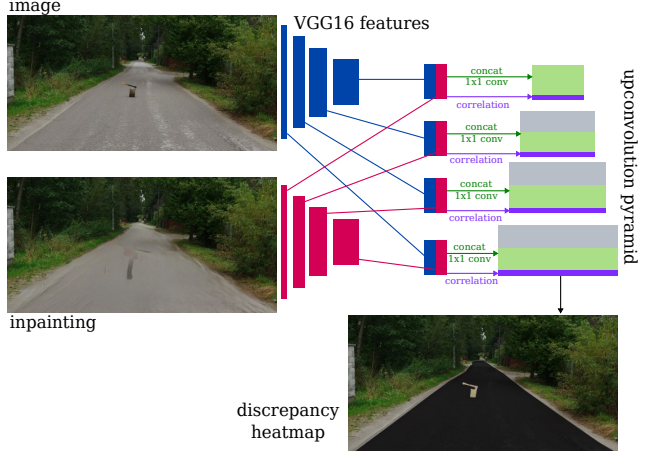


Figure 4. **Architecture of the discrepancy network**

where s is the patch width or height and $\Pi(u, v)$ is the set of patches overlapping the $[u, v]^\top$ pixel, with patch i centered at $[u_i, v_i]$.

3.2. Discrepancy Network

While our inpainting strategy preserves the general appearance of the road surface, it still yields unavoidable imperfections due to road markings, texture details, and the non-zero contributions of obstacles located close to the patch edges. Thus, simply comparing the original image with the inpainted one via pixel difference would yield many false positive detections. To handle this, we introduce a *discrepancy network* that we train to distinguish significant differences from inpainting artifacts.

We implement our discrepancy network using a two-stream architecture, shown in Fig. 4, that takes as input the original image and the inpainted one. Both inputs are first processed by a VGG [42] feature extractor. The resulting features are then concatenated and fused through 1×1 convolutions. Furthermore, we compute a point-wise correlation map of the image and inpainting features, which we append as an additional channel to the output of the 1×1 convolutions. The concatenated features are then passed to an upconvolution pyramid, and we obtain the desired heatmap via a softmax.

3.2.1 Training the Discrepancy Network

Recall that we target unusual road obstacles that may never have been seen at training time. Therefore, we need the discrepancy network to generalize to previously-unseen objects.

To tackle this challenge, we built a synthetic training set from only the Cityscapes [10] dataset, which

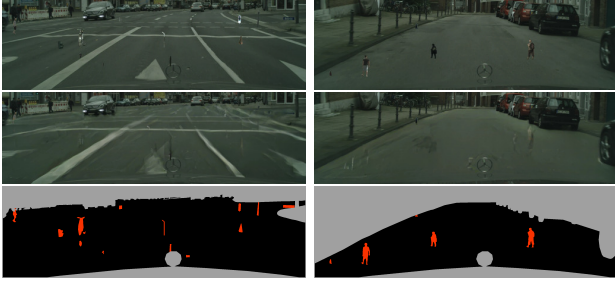


Figure 5. **Synthetic training obstacles.** Using the Cityscapes dataset, we transplant random object instances onto the road to appear as small obstacles (top). Results of the inpainting process (middle). Labels (bottom): the discrepancy network is trained to distinguish obstacles (red) from the road area (black), while the background grey region is ignored in training.



Figure 6. **Incorporating noise.** We augment the training images (left) by adding noise summed at two scales and magnitudes (right) to simulate a diverse road texture and prevent the discrepancy network from becoming excessively sensitive to high frequencies.

contains no unusual traffic obstacles. We extracted instances of people and vehicles using the instance annotations, together with *traffic lights* and *traffic signs*, which lack instance labels, but can be extracted as connected components within their pixel-wise semantic label mask. Since many road obstacles are small and difficult to detect, to simulate small obstacles seen from a far distance, we selected from the whole dataset instances of size ranging from 10 to 150 pixels, and area between 100 and 5000 pixel squared. We then sampled random objects from this database and overlaid them onto the drivable area to mimic obstacles. Fig. 5 features several images synthesized in this way.

3.2.2 High-frequency Appearance Variations

Our approach to overlaying synthetic obstacles on real roads introduces sharp discontinuities in our training images. This makes the discrepancy network over-sensitive to high-frequency appearance variations, leading to false positives in test images depicting road surfaces rougher than the Cityscapes ones. We address this issue by first applying a Gaussian blur to the train-

ing images and then adding noise at two different scales to them to create a more realistic texture, as shown in Fig. 6. We also blur the input images at test time. We will evaluate the influence of this step in Section 4.5. We do not blur the inpainted image since our patch fusion strategy already tends to smooth it.

4. Experiments

In this section, we first present the baselines, evaluation metrics, and datasets used in our experiments. We then compare our approach to the baselines and finally perform an ablation study.

4.1. Baselines

We compare against the following approaches.

Resynthesis [28] performs semantic segmentation of the image and then synthesizes an image solely from the resulting semantic map using a conditional GAN [45]. The differences between the original and reconstructed images are detected using a discrepancy network similar in purpose to the one we use, but trained by synthetically swapping Cityscapes object classes.

Discriminative Outlier Detection Head [3] relies on an outlier detection head that shares backbone features with a semantic segmentation head. The network is trained using frames from Cityscapes and Vis-tas [35], with injected outliers drawn from ImageNet-1k [12]. We evaluate a variant where outlier size is randomized in order to handle a range of obstacle sizes.

Learned Embedding Density [5] learns the inlier distribution of features extracted from a DeepLab [7] layer. It then maps the features to latent, Gaussian-distributed vectors via a normalizing flow. The mapping is trained to maximize the likelihood of the features observed in inlier samples.

DeepLab Softmax Entropy [26] measures the entropy of the class likelihoods produced by the softmax layer of the DeepLab semantic segmentation network.

OoD Training [26] uses the Cityscapes *void* areas as examples of outliers. It can then either explicitly add *void* to the set of predicted classes, or learn to maximize the softmax entropy in the *void* regions.

Bayesian DeepLab [31] introduces dropout layers into the DeepLab network. At inference time, it draws samples by randomizing the dropout. The uncertainty is measured as the mutual information between the resulting distribution and the network weights.

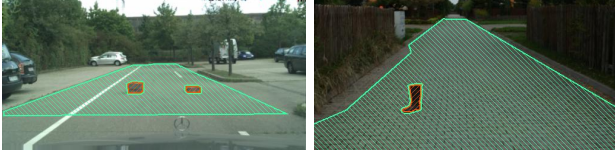


Figure 7. **Example ground-truth labels.** We consider the task of distinguishing obstacle pixels (orange) from the road area (light green), while the background (unmarked) is excluded from the evaluation.

Dirichlet DeepLab [30] outputs the α parameters defining a Dirichlet distribution over the class labels, rather than a single set of class likelihoods given by the softmax. The network is trained to produce sharp distributions for inlier classes and a uniform distribution for the *void* class. The anomaly score is calculated as the Dirichlet differential entropy.

4.2. Evaluation Metrics

Since we focus on detecting obstacles on the road, we take the Region of Interest (ROI) for evaluation purposes to be the ground-truth road area as shown in Fig. 7. We formulate our task in terms of pixel-wise binary classification. Our method, like the baselines we compare with, outputs a heatmap in the $[0, 1]$ range denoting the likelihood for each pixel within the ROI of belonging to an obstacle. We use the following two metrics of the *Fishyscapes* benchmark [5]:

- The primary metric is Average Precision (AP), that is, the area under the precision-recall curve. This metric is more meaningful than metrics based on the receiver operating curve (ROC) due to strong class imbalance, as obstacles typically cover less than 2% of the total road surface.
- A secondary metric is false positive rate (FPR) at a 95% true positive rate (TPR), which we denote as FPR_{95} . To compute it, the binary classification threshold is lowered until 95% of the obstacle pixels are detected and we then measure how many false positives are introduced.

4.3. Datasets

We report empirical results on two datasets, the well-established *Fishyscapes Lost & Found* benchmark and a new *Road Obstacles* dataset that we introduce in this paper to increase the diversity of road obstacles and surfaces.

Fishyscapes Lost & Found. The Lost & Found dataset [36] contains image sequences captured by a vehicle approaching lost cargo items placed on parking lots and streets. A subset of 100 validation and

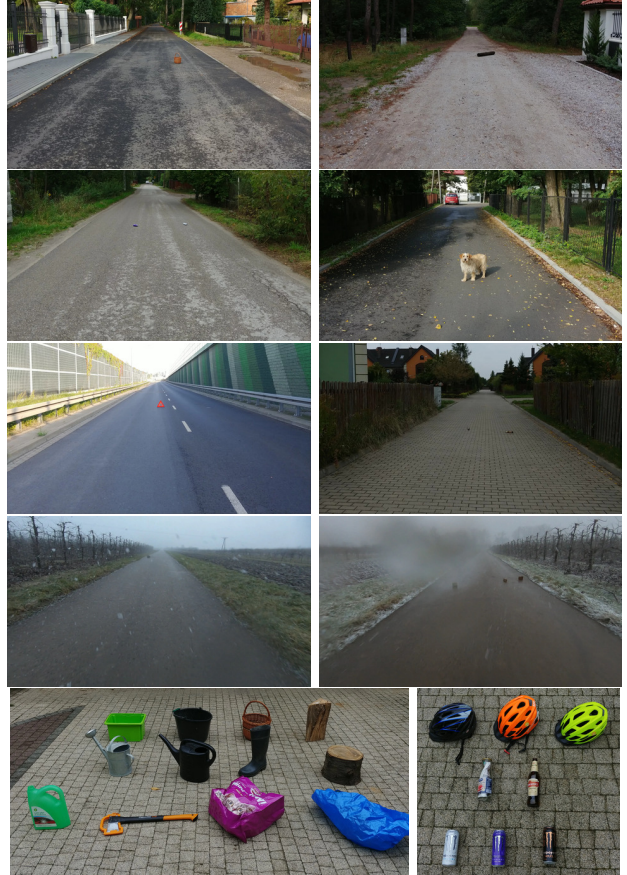


Figure 8. **Road Obstacles dataset.** Top: Example frames representing each of the 7 scenes. Bottom: Some of the objects featured in the dataset.

275 test images was selected from the *Fishyscapes* [5] road scene anomaly detection benchmark to avoid non-anomalous Cityscapes objects, such as people. We adapted the benchmark to the task of obstacle detection on known road regions by restricting the evaluation to the ground-truth labeled drivable area. This was done in close collaboration with the *Fishyscapes* benchmark organizers. They will integrate this evaluation strategy in the benchmark but are neither authors of this paper nor associated to the corresponding research. The results of the baseline methods were computed by them, using the original implementations submitted to the benchmark that were presumably tuned by their respective authors for the benchmark and its Lost&Found part.

We evaluate both with the publicly available validation set and the private test set. Scores for the latter were computed by the benchmark authors and given to us. They are consistent with those we obtained on the validation set.

Road Obstacles The *Lost & Found* benchmark features urban environments similar to those in the *Cityscapes* training data. To evaluate our obstacle detector on a wider variety of road surfaces and objects, we collected our own *Road Obstacles* dataset, which is depicted by Fig. 8. It features seven different scenes and comprises a total of 160 labeled 1920×1080 frames. The labels include pixel masks for individual obstacle instances along with approximate outlines of the drivable area. We take the evaluation ROI to be the area within these outlines. If an object has a hole, such as a basket with a handle, we label the hole as outside of the ROI and ignore it in our evaluations, as we do for the background.

Below we present scores for the six scenes with good daylight visibility. In the supplementary material, we provide an additional evaluation using images taken in more difficult weather conditions.

4.4. Comparative Results

We tested two versions of our method, one that operates on the road area given in the ground truth and the other on the drivable area segmented by the network of [51]. They are referred to as “Ours road ground truth” and “Ours road segmentation”, respectively, in Table 1.

Both versions of our method outperform all others in terms Average Precision (AP), the primary metric in [5], on both datasets. The same is true for the FPR₉₅, the secondary metric, except for “Ours road segmentation” on the test set of Fishyscapes for which our FPR score is abysmal. Note, however, that the score using the ground truth is excellent. This points to the cause of the problem: The segmentation algorithm we use only found a part of the drivable area and, since we only look for obstacles there, we missed all those that were elsewhere, making it impossible to reach a 95% TPR in some of the images. Fig. 9 illustrates this problem. Nevertheless, even in this situation, safety is maintained because the vehicle controller will only drive within the predicted road space. Hence, obstacles outside of it do not pose a risk of collision. Furthermore, as evidenced by the excellent results of “Ours road ground truth”, this problem will gradually fade away as road boundary detection algorithms improve.

4.5. Ablation study

In Table 2, we report the results of an ablation study during which the discrepancy network was retrained with selected components altered or disabled.

In the *Resynthesis* variant, the inpainting described in Section 3.1 is replaced by an image synthesizer [45]

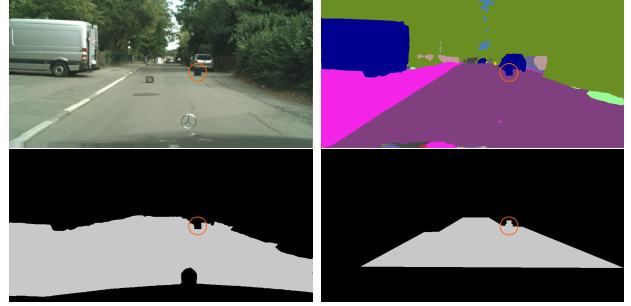


Figure 9. **Obstacle outside of predicted drivable area failure mode.** **Top-left:** An obstacle is located near a vehicle shadow. **Top-right:** The semantic segmenter classifies it as part of the background. **Bottom-left:** Consequently it is not included in the drivable space where our obstacle detector is applied. **Bottom-right:** Ground truth road label used as the region-of-interest for evaluation purposes. This obstacle will be counted as missed.

from predicted semantic labels as in [28]. While the inpainter can reconstruct novel road textures based on the visual context, the generator produces a texture similar to the training roads, and this is reflected by degraded performance on *Road Obstacles*.

The *No Inpainting* variant does away with inpainting. We keep the architecture unchanged, but pass two copies of the image into both input streams. This also degrades performance, thus confirming the importance of inpainting. We can also do the reverse, that is, remove the discrepancy network, and compute the L_1 distance between the RGB values of the input image and the inpainted result. The results of the corresponding *No Discrepancy* variant are even worse.

The *Segmentation Alone* entry corresponds to detections made by finding groups of non-road pixels enclosed within the road region detected by the segmentation algorithm [51]. This by itself clearly fails, thereby justifying the extra step we propose in this paper.

Finally, recall from Section 3.2.2 that we add noise to the training images to prevent overfitting to smooth road surfaces and further blur the images. Turning this off in *Ours w/o noise aug.* and *Ours w/o blur.* degrades performance on Road Obstacles, which features rough roads, but slightly improves it on Fishyscapes, where the roads are indeed mostly smooth. In other words, we trade some accuracy on well paved roads for resiliency on rougher ones.

5. Conclusion

We have introduced a pipeline capable of detecting road obstacles in driving scenarios, given only single monocular images as input. We perform inpainting of the drivable area, erasing the localized obstacles

Method		Road Obstacles daylight		Fishyscapes: L&F validation		Fishyscapes: L&F test	
		AP \uparrow	FPR ₉₅ \downarrow	AP \uparrow	FPR ₉₅ \downarrow	AP \uparrow	FPR ₉₅ \downarrow
Ours	road ground truth	85.4	1.8	88.7	2.2	91.3	1.0
Ours	road segmentation	84.7	2.3	87.0	3.1	84.8	99.1
Outlier Detection Head [3]	random sized patches	70.8	0.9	61.4	27.0	53.1	36.1
Resynthesis [28]	discrepancy network	34.5	4.1	64.4	5.1	67.0	6.0
Dirichlet DeepLab [30]	prior entropy	11.7	31.6	61.2	70.8	59.9	73.0
Learned Embedding	minimum NLL	2.3	27.8	61.1	8.5	71.7	6.7
Density [5]	single-layer NLL	1.0	62.0	49.6	17.2	55.8	13.6
Bayesian DeepLab [31]	mutual information	13.0	49.1	48.4	33.7	41.3	30.6
DeepLab Softmax [26]	entropy	26.2	10.9	29.4	41.0	27.5	29.4
OoD training	void classifier	8.7	48.6	14.1	24.2	4.7	41.0

Table 1. **Obstacle detection scores.** The primary metric is *average precision* of detecting obstacle pixels.

	Road Obstacles daylight		Fishyscapes: L&F validation		Fishyscapes: L&F test	
	AP \uparrow	FPR ₉₅ \downarrow	AP \uparrow	FPR ₉₅ \downarrow	AP \uparrow	FPR ₉₅ \downarrow
Ours	84.7	2.3	87.0	3.1	84.8	99.1
Resynthesis.	69.9	8.4	75.6	5.4	68.2	99.9
No Inpainting.	81.9	2.8	84.8	2.9	82.6	97.5
No Discrepancy	15.3	40.2	21.1	48.4	23.1	84.8
Segmentation Alone	13.4	85.1	34.4	91.8	42.6	91.2
Ours w/o noise aug.	77.7	14.8	86.8	3.1	85.0	82.8
Ours w/o blur.	80.5	2.2	87.7	4.2	86.0	85.7

Table 2. **Ablation study results.**

while preserving the road surface. Our discrepancy network learns to accurately detect the removed obstacles and ignore irrelevant artifacts of reconstruction. This detector, trained only with synthetically altered Cityscapes data, is capable of generalizing to a variety of real-world obstacles and road surfaces. We have demonstrated this on the *Fishyscapes Lost & Found* benchmark, as well as on our newly collected dataset. We will release our dataset to the community to help researchers in this field.

In the future, we will work on coupling more tightly the algorithms that detect the drivable area and ours for improved results and for potential integration into a full self-driving system. We also plan to exploit adaptive inpainting patch sizes to account for perspective distortion.

Acknowledgements

We thank **Hermann Blum** for adapting the Fishyscapes benchmark and baseline methods to our data as well as help with the evaluations. We thank **Miroslaw Lis** for assistance in the collection of the *Road Obstacles* dataset.

References

- [1] AutoNation Drive Editors’ Guide to Lane Assist Systems. <https://www.autonationdrive.com/research/best-cars-with-lane-assist.htm>. accessed March 2021. **1**
- [2] S. Akcay, A. Atapour-Abarghouei, and T. P. Breckon. Ganomaly: Semi-Supervised Anomaly Detection via Adversarial Training. In *Asian Conference on Computer Vision*, 2018. **2**
- [3] P. Bevandić, I. Krešo, M. Oršić, and S. Šegvić. Simultaneous Semantic Segmentation and Outlier Detection in Presence of Domain Shift. In *German Conference on Pattern Recognition*, 2019. **2, 5, 8, 12**
- [4] A. Bhattad, J. Rock, and D. Forsyth. Detecting Anomalous Faces with ‘No Peeking’ Autoencoders. In *Conference on Computer Vision and Pattern Recognition*, 2018. **1**
- [5] H. Blum, P.-E. Sarlin, J. Nieto, R. Siegwart, and C. Cadena. Fishyscapes: A Benchmark for Safe Semantic Segmentation in Autonomous Driving. In *International Conference on Computer Vision*, October 2019. **2, 3, 5, 6, 7, 8, 12**
- [6] Florian Chabot, Mohamed Chaouch, Jaonary Rabarisoa, Céline Teulière, and Thierry Chateau. Deep manta: A coarse-to-fine many-task network for joint 2d and 3d vehicle analysis from monocular

- image. In *Conference on Computer Vision and Pattern Recognition*, 2017. 1
- [7] L. Chen, G. Papandreou, I. Kokkinos, K. Murphy, and A. L. Yuille. Deeplab: Semantic Image Segmentation with Deep Convolutional Nets, Atrous Convolution, and Fully Connected CRFs. *IEEE Transactions on Pattern Analysis and Machine Intelligence*, 2018. 5
- [8] L.-C. Chen, G. Papandreou, F. Schroff, and H. Adam. Rethinking Atrous Convolution for Semantic Image Segmentation. In *arXiv Preprint*, 2017. 1
- [9] Zhe Chen and Zijing Chen. RBNet: A Deep Neural Network for Unified Road and Road Boundary Detection. In *International Conference on Neural Information Processing*, 2017. 1
- [10] M. Cordts, M. Omran, S. Ramos, T. Rehfeld, M. Enzweiler, R. Benenson, U. Franke, S. Roth, and B. Schiele. The Cityscapes Dataset for Semantic Urban Scene Understanding. In *Conference on Computer Vision and Pattern Recognition*, 2016. 2, 3, 4, 11
- [11] C. Creusot and A. Munawar. Real-Time Small Obstacle Detection on Highways Using Compressive RBM Road Reconstruction. In *Intelligent Vehicles Symposium*, 2015. 2
- [12] J. Deng, W. Dong, R. Socher, L.-J. Li, K. Li, and L. Fei-Fei. Imagenet: A Large-Scale Hierarchical Image Database. In *Conference on Computer Vision and Pattern Recognition*, 2009. 2, 5
- [13] P. Dollár, C. Wojek, B. Schiele, and P. Perona. Pedestrian Detection: An Evaluation of the State of the Art. *IEEE Transactions on Pattern Analysis and Machine Intelligence*, 34(4):743–761, 2012. 1
- [14] Jian Guo, He He, Tong He, Leonard Lausen, Mu Li, Haibin Lin, Xingjian Shi, Chenguang Wang, Junyuan Xie, Sheng Zha, Aston Zhang, Hang Zhang, Zhi Zhang, Zhongyue Zhang, Shuai Zheng, and Yi Zhu. Gluoncv and gluonnlp: Deep learning in computer vision and natural language processing. *Journal of Machine Learning Research*, 21(23):1–7, 2020. 11
- [15] A. Gupta, J. Johnson, L. Fei-Fei, S. Savarese, and A. Alahi. Social GAN: Socially Acceptable Trajectories with Generative Adversarial Networks. In *Conference on Computer Vision and Pattern Recognition*, 2018. 2
- [16] F. K. Gustafsson, M. Danelljan, and T. B. Schön. Evaluating Scalable Bayesian Deep Learning Methods for Robust Computer Vision. In *Conference on Computer Vision and Pattern Recognition*, 2020. 3
- [17] M. Haselmann, D. P. Gruber, and P. Tabatabai. Anomaly Detection Using Deep Learning Based Image Completion. In *International Conference on Machine Learning*, 2018. 1, 2
- [18] K. He, G. Gkioxari, P. Dollár, and R. B. Girshick. Mask R-CNN. In *International Conference on Computer Vision*, 2017. 1
- [19] P. Isola, J. Zhu, T. Zhou, and A. Efros. Image-To-Image Translation with Conditional Adversarial Networks. In *arXiv Preprint*, 2016. 2
- [20] A. Kendall, V. Badrinarayanan, and R. Cipolla. Bayesian Segnet: Model Uncertainty in Deep Convolutional Encoder-Decoder Architectures for Scene Understanding. In *arXiv Preprint*, 2015. 3
- [21] A. Kendall and Y. Gal. What Uncertainties Do We Need in Bayesian Deep Learning for Computer Vision? In *Advances in Neural Information Processing Systems*, 2017. 3
- [22] D. P. Kingma and J. Ba. Adam: A Method for Stochastic Optimisation. In *International Conference on Learning Representations*, 2015. 12
- [23] Alexander Kirillov, Kaiming He, Ross Girshick, Carsten Rother, and Piotr Dollár. Panoptic Segmentation. In *Conference on Computer Vision and Pattern Recognition*, 2019. 1
- [24] G. Klambauer, T. Unterthiner, A. Mayr, and S. Hochreiter. Self-Normalizing Neural Networks. In *Advances in Neural Information Processing Systems*, 2017. 11
- [25] B. Lakshminarayanan, A. Pritzel, and C. Blundell. Simple and Scalable Predictive Uncertainty Estimation Using Deep Ensembles. In *Advances in Neural Information Processing Systems*, 2017. 3
- [26] K. Lee, H. Lee, K. Lee, and J. Shin. Training Confidence-Calibrated Classifiers for Detecting Out-Of-Distribution Samples. In *International Conference on Learning Representations*, 2018. 5, 8, 12
- [27] W. Li, O. H. Jafari, and C. Rother. Deep Object Co-Segmentation. In *Asian Conference on Computer Vision*, 2018. 11
- [28] K. Lis, K. Nakka, M. Salzmann, and P. Fua. Detecting the Unexpected via Image Resynthesis. In *International Conference on Computer Vision*, 2019. 2, 5, 7, 8, 11, 12
- [29] Ruijin Liu, Zejian Yuan, Tie Liu, and Zhiliang Xiong. End-to-end lane shape prediction with transformers. In *IEEE Winter Conference on Applications of Computer Vision*, pages 3694–3702, 2021. 1
- [30] A. Malinin and M. Gales. Predictive Uncertainty Estimation via Prior Networks. In S. Bengio, H. Wallach, H. Larochelle, K. Grauman, N. Cesa-Bianchi, and R. Garnett, editors, *Advances in Neural Information Processing Systems*. 2018. 2, 3, 6, 8, 12
- [31] J. Mukhoti and Y. Gal. Evaluating Bayesian Deep Learning Methods for Semantic Segmentation. In *arXiv Preprint*, 2018. 5, 8, 12
- [32] A. Munawar and C. Creusot. Structural Inpainting of Road Patches for Anomaly Detection. In *IAPR International Conference on Machine Vision Applications*, 2015. 2
- [33] A. Munawar, P. Vinayavekhin, and G. De Magistris. Limiting the Reconstruction Capability of Generative Neural Network Using Negative Learning. In *IEEE International Workshop on Machine Learning for Signal Processing*, 2017. 2
- [34] Jesús Muñoz-Bulnes, Carlos Fernandez, Ignacio Parra, David Fernández-Llorca, and Miguel A Sotelo. Deep

- fully convolutional networks with random data augmentation for enhanced generalization in road detection. In IEEE International Conference on Intelligent Transportation Systems (ITSC), 2017. [1](#)
- [35] Gerhard Neuhold, Tobias Ollmann, Samuel Rota Bulo, and Peter Kotschieder. The Mapillary Vistas Dataset for Semantic Understanding of Street Scenes. In Conference on Computer Vision and Pattern Recognition, 2017. [2](#), [5](#)
- [36] P. Pinggera, S. Ramos, S. Gehrig, U. Franke, C. Rother, and R. Mester. Lost and Found: Detecting Small Road Hazards for Self-Driving Vehicles. In International Conference on Intelligent Robots and Systems, 2016. [1](#), [2](#), [6](#), [12](#)
- [37] Zequn Qin, Huanyu Wang, and Xi Li. Ultra Fast Structure-aware Deep Lane Detection. In European Conference on Computer Vision, 2020. [1](#)
- [38] S. Ramos, S. Gehrig, P. Pinggera, U. Franke, and C. Rother. Detecting Unexpected Obstacles for Self-Driving Cars: Fusing Deep Learning and Geometric Modeling. In IEEE Intelligent Vehicles Symposium, 2017. [2](#)
- [39] S. Ren, K. He, R. Girshick, and J. Sun. Faster R-CNN: Towards Real-Time Object Detection with Region Proposal Networks. In Advances in Neural Information Processing Systems, 2015. [1](#)
- [40] Eduardo Romera, José M Alvarez, Luis M Bergasa, and Roberto Arroyo. ERFNet: Efficient Residual Factorized ConvNet for Real-time Semantic Segmentation. IEEE Transactions on Intelligent Transportation Systems, 2017. [1](#)
- [41] T. Schlegl, P. Seeböck, S. M. Waldstein, U. Schmidt-Erfurth, and G. Langs. Unsupervised Anomaly Detection with Generative Adversarial Networks to Guide Marker Discovery. In International Conference on Information Processing in Medical Imaging, 2017. [2](#)
- [42] K. Simonyan and A. Zisserman. Very Deep Convolutional Networks for Large-Scale Image Recognition. In International Conference on Learning Representations, 2015. [4](#), [11](#)
- [43] Aasheesh Singh, Aditya Kamireddypalli, Vineet Gandhi, and K Madhava Krishna. LiDAR guided Small obstacle Segmentation. arXiv preprint arXiv:2003.05970, 2020. [1](#)
- [44] N. Srivastava, G. Hinton, A. Krizhevsky, I. Sutskever, and R. Salakhutdinov. Dropout: A Simple Way to Prevent Neural Networks from Overfitting. Journal of Machine Learning Research, 15:1929–1958, 2014. [3](#)
- [45] T.-C. Wang, M.-Y. Liu, J.-Y. Zhu, A. Tao, J. Kautz, and B. Catanzaro. High-Resolution Image Synthesis and Semantic Manipulation with Conditional GANs. In Conference on Computer Vision and Pattern Recognition, 2018. [2](#), [5](#), [7](#)
- [46] Y. Xia, Y. Zhang, F. Liu, W. Shen, and A. Yuille. Synthesize Then Compare: Detecting Failures and Anomalies for Semantic Segmentation. In European Conference on Computer Vision, 2020. [2](#)
- [47] Yuwen Xiong, Renjie Liao, Hengshuang Zhao, Rui Hu, Min Bai, Ersin Yumer, and Raquel Urtasun. UPSNet: A Unified Panoptic Segmentation Network. In Conference on Computer Vision and Pattern Recognition, 2019. [1](#)
- [48] F. Xue, A. Ming, M. Zhou, and Y. Zhou. A Novel Multi-Layer Framework for Tiny Obstacle Discovery. In International Conference on Robotics and Automation, 2019. [2](#)
- [49] J. Yu, Z. Lin, J. Yang, X. Shen, X. Lu, and T. S. Huang. Free-Form Image Inpainting with Gated Convolution. In Conference on Computer Vision and Pattern Recognition, 2019. [3](#)
- [50] V. Zavrtanik, M. Kristan, and D. Skočaj. Reconstruction by Inpainting for Visual Anomaly Detection. Pattern Recognition, 2020. [1](#), [2](#)
- [51] H. Zhao, J. Shi, X. Qi, X. Wang, and J. Jia. Pyramid Scene Parsing Network. In Conference on Computer Vision and Pattern Recognition, 2017. [1](#), [3](#), [7](#), [11](#)
- [52] B. Zhou, A. Lapedriza, A. Khosla, A. Oliva, and A. Torralba. Places: A 10 Million Image Database for Scene Recognition. IEEE Transactions on Pattern Analysis and Machine Intelligence, 2017. [4](#)

Appendices

Fig. 12, Fig. 13 and Fig. 14 depict our results qualitatively. The ROC and precision-recall curves for the obstacle pixel classification are shown in Fig. 16, Fig. 17, Fig. 18 and Fig. 19.

A. Difficult weather

As part of our dataset we have collected 55 frames taken during a snowfall. They pose additional challenges for the obstacle detector: snowflakes visible in the air can trigger false positives, and a water drop on the camera lens can obscure parts of an image. Images of the *snowfall* sequence are shown in Fig. 14.

We report the *snowfall* track separately, as such conditions are far outside the training domains of any of the evaluated methods. In Table 3 we present the detection scores for the main 105-frame *daylight* subset, the 55-frame *snowfall* subset and the combination of *all* frames. The corresponding detection curves are shown in Fig. 16 and Fig. 17. The difficult weather causes nearly all baselines to fail, but our approach maintains reasonable performance.

Table 4 contains the results of the ablation study for the subsets of our dataset. Unlike in the *daylight* scenes, the noise augmentation and input blurring are detrimental to our method’s performance in difficult weather conditions. This indicates there is no single solution to domain-shift, and future work in this direction is warranted.

B. Implementation details

In this section, we present details on drivable area selection and discrepancy network architecture and training.

B.1. Determining the drivable area

Our method detects obstacles within the drivable area, as these are the ones posing a danger to the vehicle. Our approach can work with any source that provides drivable area information.

In our experiments, we use the PSP-Net semantic segmentation network of [51] trained on the Cityscapes dataset [10], as implemented in the framework of [14]. We take the road area to be all pixels classified as either *road* or *sidewalk*, since the diverse road textures we are targeting can be classified as either. Note that standard categories, such as *car* and *pedestrian*, are inherently accounted for by PSP-Net; we then focus on the unusual obstacles for which no training data, neither supervised not unsupervised, is available. Nevertheless, since such unusual obstacles could be partially

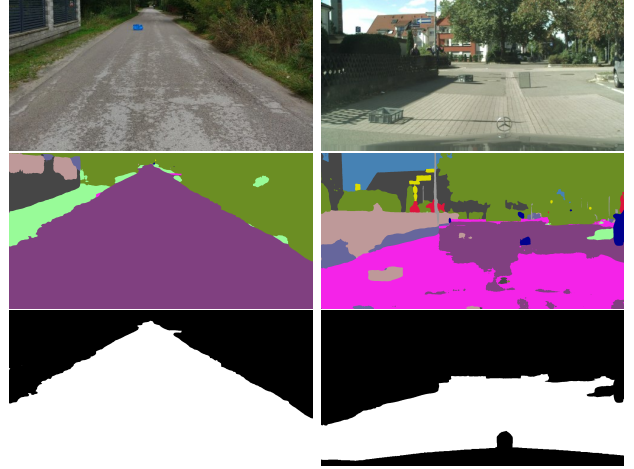


Figure 10. **Drivable space from semantic segmentation.** **Top:** Input images. **Middle:** Semantic segmentation performed by PSP-Net [51], the class colors follow Cityscapes convention. **Bottom:** We take the drivable space to be the union of *road* (purple) and *sidewalk* (magenta) pixels. The parts of obstacles can sometimes be classified as non-road, so we include the regions of other classes fully enclosed within the road area. In *Lost & Found*, the known ego-vehicle mask is excluded.

classified as non-road, we include the regions containing other classes that are fully enclosed within the road area. Examples outputs of the process are shown in Fig. 10.

B.2. Discrepancy Network Architecture

We use the discrepancy network architecture of [28] but without the semantic branch, since we aim for compatibility with non-semantic free-space estimation methods. The architecture is shown in Fig. 15.

The network has two input streams: the original image and the image where the road area has been inpainted. We apply Gaussian blur to the input image to eliminate excessive high-frequency signals, as described in the main article. We use the pretrained VGG network of [42] to extract features from both images. At four levels of the feature pyramid, we fuse the two streams of features in these two parallel ways:

- Concatenate stream 1 and 2, followed by a 1×1 convolution,
- Calculate pixel-wise correlation of features, following [27].

The results of the above are concatenated and passed on to an up-convolution pyramid which uses the SeLU [24] activation function. In the final step, the discrepancy score is multiplied by the binary drivable

Method		Road Obstacles daylight		Road Obstacles snowfall		Road Obstacles all	
		AP \uparrow	FPR ₉₅ \downarrow	AP \uparrow	FPR ₉₅	AP \uparrow	FPR ₉₅
Ours	road ground truth	85.4	1.8	54.6	11.1	81.2	3.6
Ours	road segmentation	84.7	2.3	55.3	10.8	81.9	3.7
Outlier Detection Head [3]	random sized patches	70.8	0.9	0.7	54.0	30.4	5.0
Resynthesis [28]	discrepancy network	34.5	4.1	19.2	15.0	31.9	5.9
Dirichlet DeepLab [30]	prior entropy	11.7	31.6	0.6	45.5	4.8	37.8
Learned Embedding	minimum NLL	2.3	27.8	0.9	38.6	2.1	33.7
Density [5]	single-layer NLL	1.0	62.0	0.1	84.1	0.9	71.2
Bayesian DeepLab [31]	mutual information	13.0	49.1	0.8	51.6	11.3	47.8
DeepLab Softmax [26]	entropy	26.2	10.9	2.9	60.9	22.6	14.1
OoD training	void classifier	8.7	48.6	2.9	22.6	10.5	41.2

Table 3. **Obstacle detection scores**, including the *snowfall* sequence. The primary metric is *average precision* of detecting obstacle pixels.

	Road Obstacles daylight		Road Obstacles snowfall		Road Obstacles all	
	AP \uparrow	FPR ₉₅ \downarrow	AP \uparrow	FPR ₉₅	AP \uparrow	FPR ₉₅
Ours	84.7	2.3	55.3	10.8	81.9	3.7
Resynthesis.	69.9	8.4	53.9	13.1	66.7	7.6
No Inpainting.	81.9	2.8	31.7	13.7	76.3	4.2
No Discrepancy	15.3	40.2	28.8	36.2	14.1	35.7
Segmentation Alone	13.4	85.1	0.3	98.2	12.9	90.6
Ours w/o noise aug.	77.7	14.8	65.7	3.8	75.2	11.3
Ours w/o blur.	71.4	9.9	60.6	2.1	70.9	7.4

Table 4. **Ablation study results**, including the *snowfall* sequence.

space mask, since the outputs are only valid within the road area.

B.3. Discrepancy Network Training

The discrepancy network was trained for 65 epochs. Each epoch iterates over the 2975 frames of our synthetic training set. The training is done using 768×384 crops of the road area. To improve training reproducibility, we pre-define the crops and their ordering in each epoch, and train all variants of the discrepancy network with the same sequence of samples.

We use binary cross entropy loss, but due to strong class imbalance between obstacles and background, the obstacle pixels’ loss contribution are weighted higher than those of background pixels. We maintain the weights set as in [28].

We use the Adam [22] optimizer. We set the initial learning rate to 10^{-4} and then adjust it dynamically, if there is no improvement of validation loss for 5 consecutive epochs, the learning rate is reduced 10 times. We generate the validation set from Cityscapes validation subset in the same way as the training set.



Figure 11. In *Lost&Found* only the central obstacles are labeled.

C. Lost&Found region of interest

When using the *Lost&Found* dataset [36], we constrain the evaluation to the area of the ground truth free-space label, and exclude the rest of the image. This region is visualized in Fig. 7 in the main article.

While it would be interesting to test the detection of other clutter objects visible in the dataset, the obstacles outside of the aforementioned free-space are not labeled. Only the central objects are labeled, leaving the off-center obstacles (trash cans, pallets, fences, poles) marked as background. For example, in Fig. 11, a wooden pallet is labeled as an obstacle when in front of the car but as background when leaning against a wall.

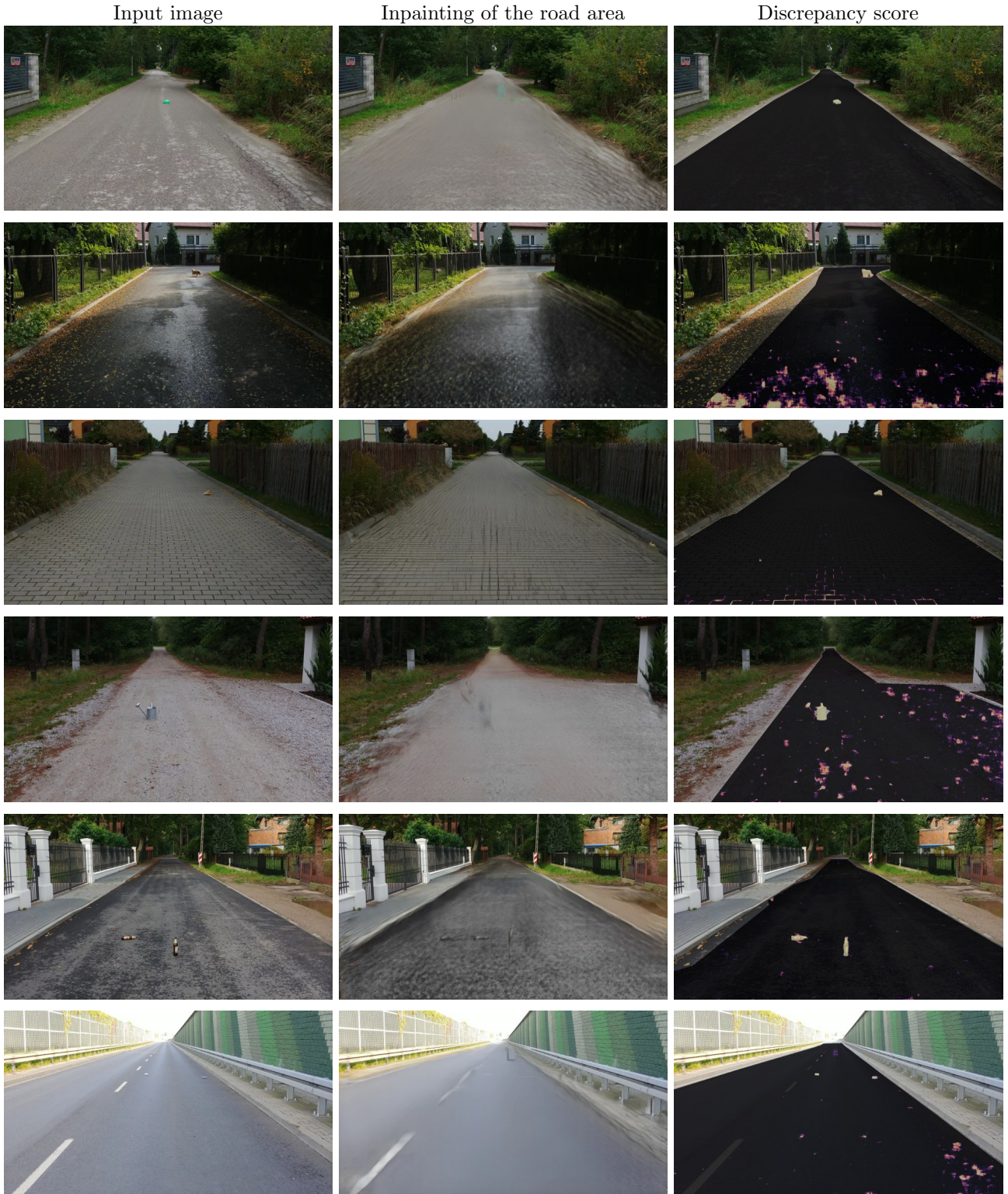


Figure 12. **Example outputs of our method for the Road Obstacles dataset. Left:** Input images featuring challenging or distant obstacles. **Center:** The result of sliding-window inpainting of the road area. **Right:** The discrepancy score calculated by our network given the two previous images. The darkened area corresponds to the ground-truth drivable space.



Figure 13. **Example outputs of our method for the Fishyscapes Lost & Found dataset.** **Left:** Input images; some of the non-drivable area has been cropped for easier viewing. **Center:** The result of sliding-window inpainting of the road area. **Right:** The discrepancy score calculated by our network given the two previous images. The darkened area corresponds to the ground-truth drivable space.

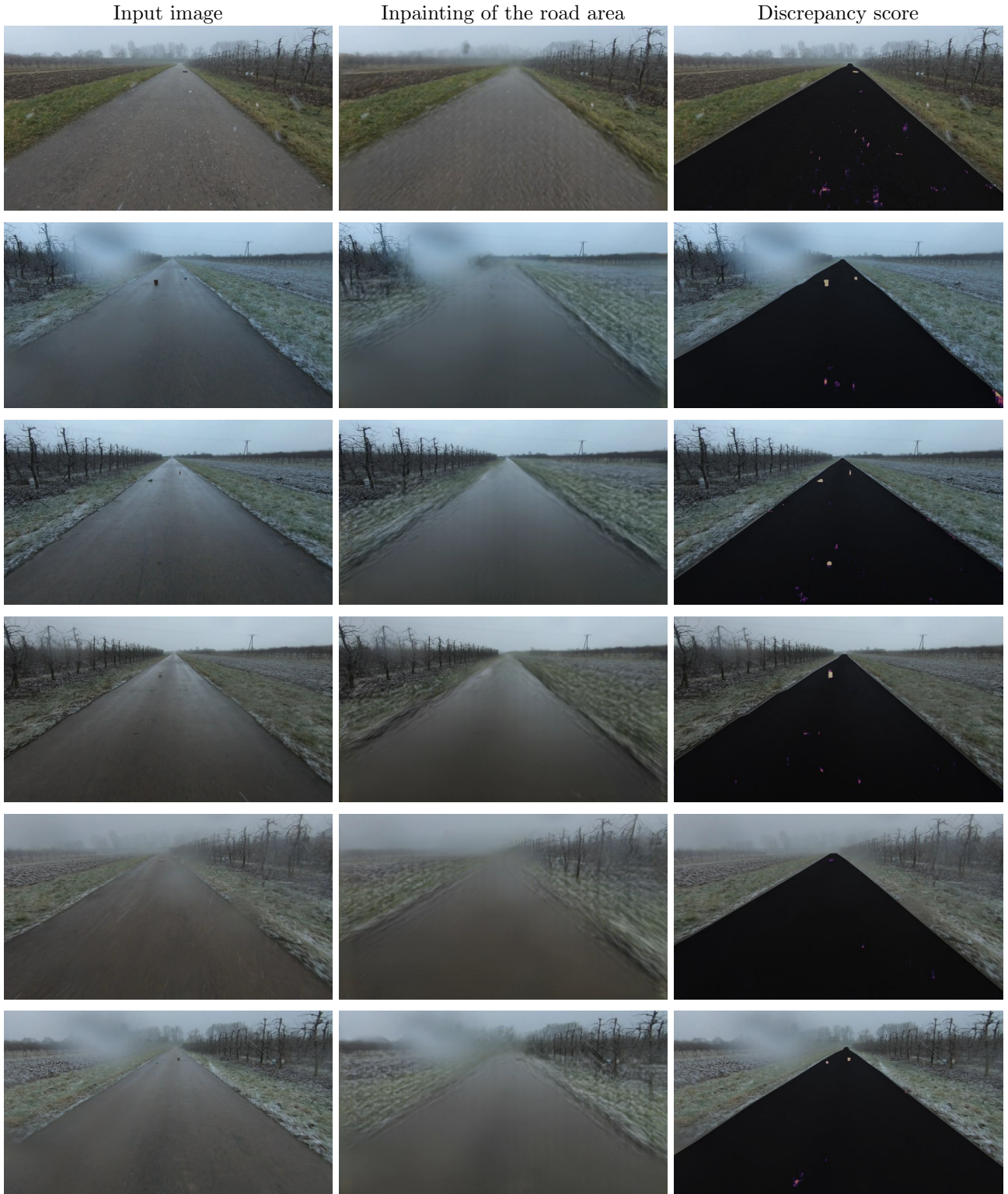


Figure 14. **Example outputs of our method for the *snowfall* subset of our Road Obstacles dataset. Left:** Input images featuring challenging or distant obstacles. **Center:** The result of sliding-window inpainting of the road area. **Right:** The discrepancy score calculated by our network given the two previous images. The darkened area corresponds to the ground-truth drivable space.

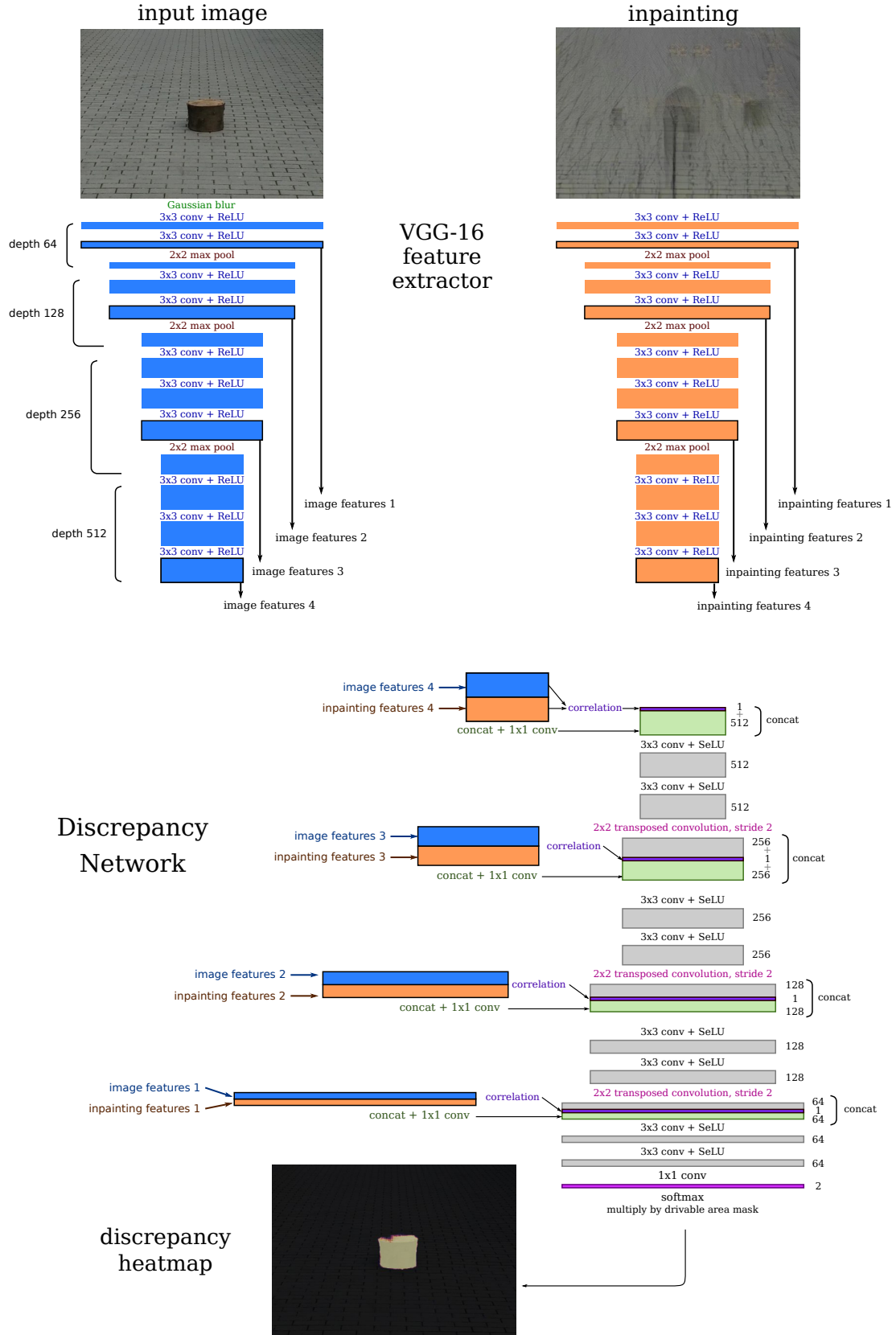


Figure 15. Discrepancy network architecture.

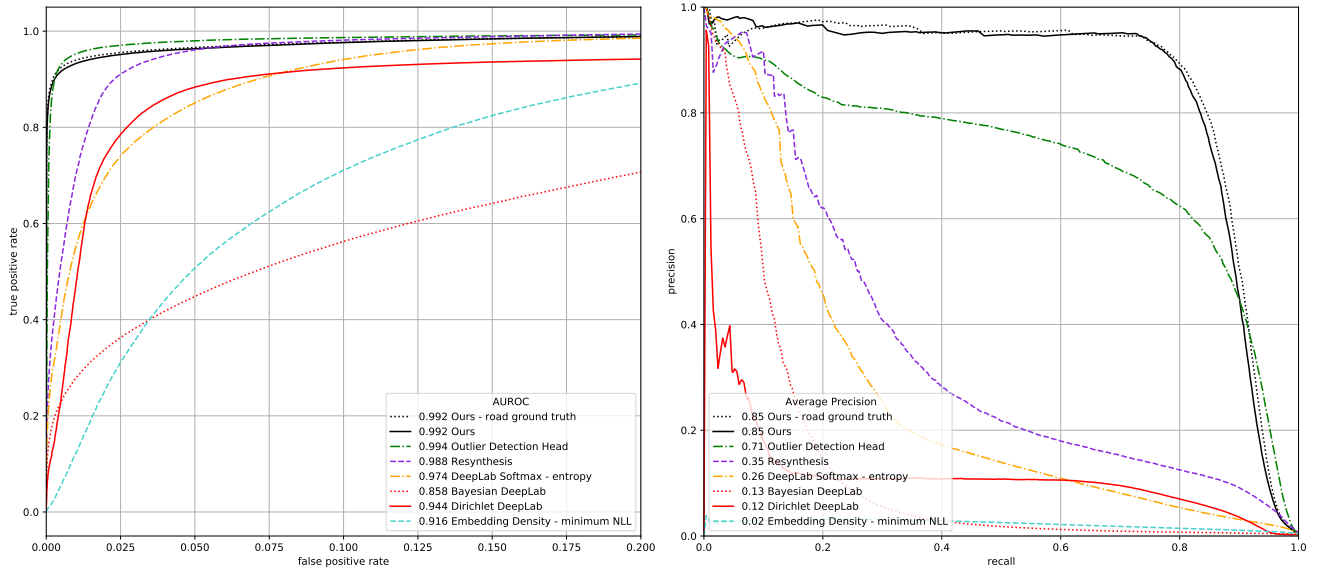


Figure 16. Obstacle detection ROC and Precision-Recall curves - Road Obstacles daylight.

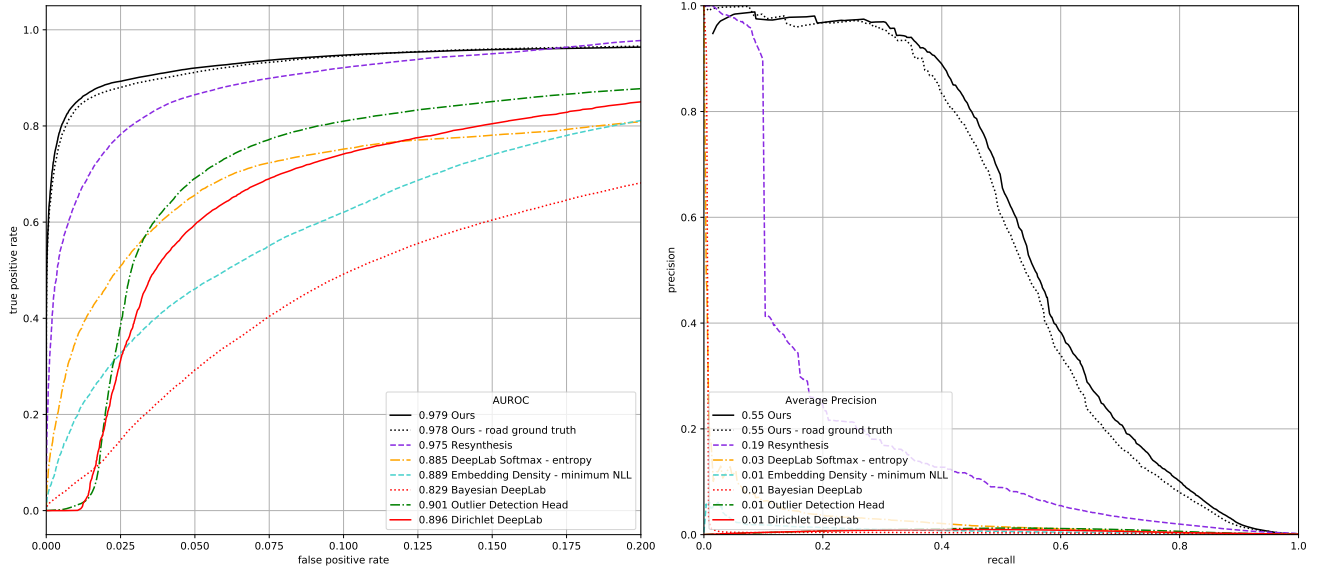


Figure 17. Obstacle detection ROC and Precision-Recall curves - Road Obstacles snowfall.

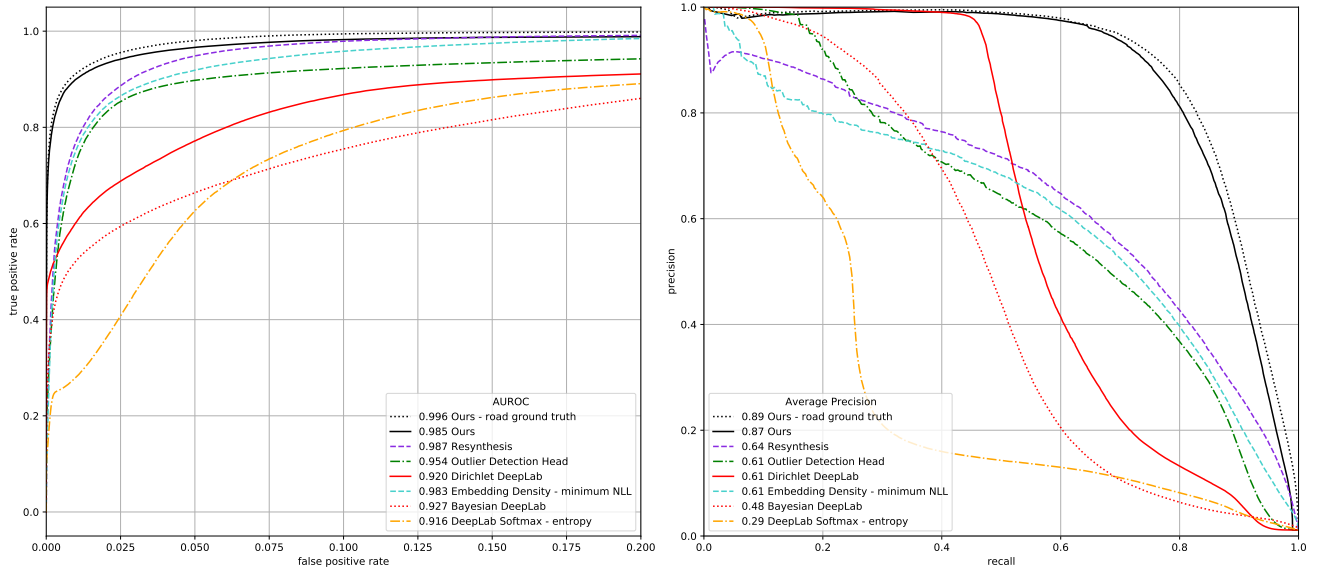


Figure 18. Obstacle detection ROC and Precision-Recall curves - Fishyscapes Lost&Found Validation.

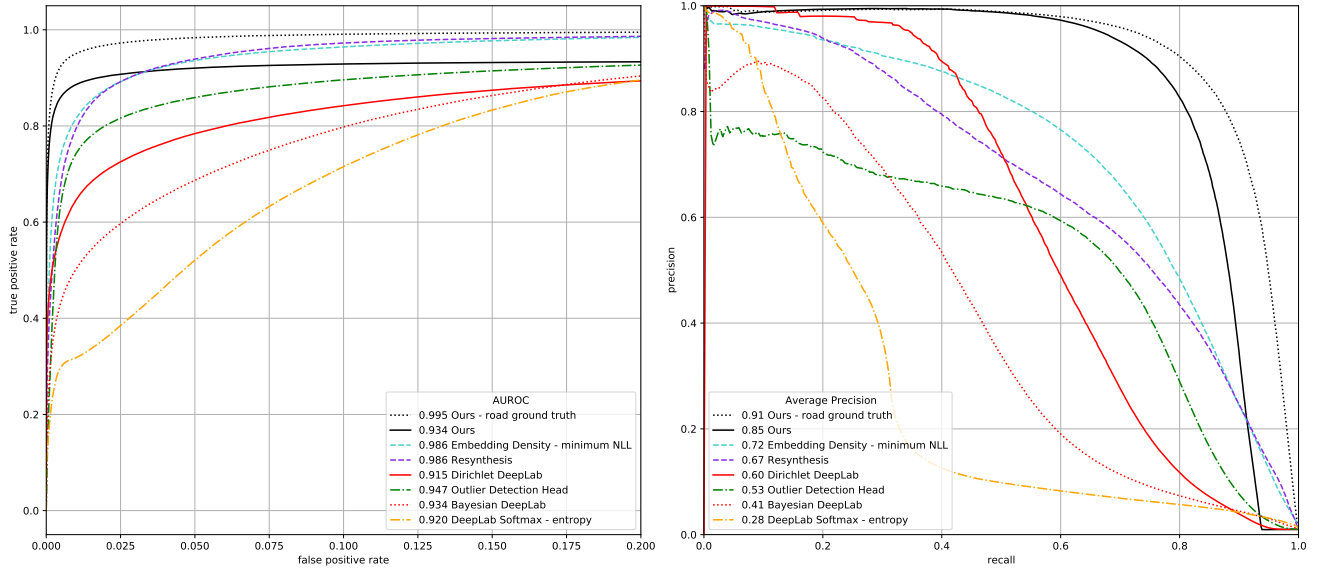


Figure 19. Obstacle detection ROC and Precision-Recall curves - Fishyscapes Lost&Found Test.